Palaeogeography, Palaeoclimatology, Palaeoecology 279 (2009) 186–200

Contents lists available at ScienceDirect

Palaeogeography, Palaeoclimatology, Palaeoecology

journal homepage: www.elsevier.com/locate/palaeo

Extinction and recovery of benthic foraminifera across the Paleocene–Eocene Thermal Maximum at the Alamedilla section (Southern Spain)

L. Alegret [a,*], S. Ortiz [a,b], E. Molina [a]

[a] Dpto. Ciencias de la Tierra (Paleontología), Facultad de Ciencias, Universidad de Zaragoza, 50009 Zaragoza, Spain
[b] Department of Earth Sciences, University College London, WC1E 6BT London, UK

ARTICLE INFO

Article history:
Received 30 December 2008
Received in revised form 25 April 2009
Accepted 10 May 2009

Keywords:
Paleocene–Eocene
Warming
Extinction
Benthic foraminifera
Deep-sea

ABSTRACT

A complete succession of lower bathyal–upper abyssal sediments was deposited across the Paleocene–Eocene Thermal Maximum (PETM) at Alamedilla (Betic Cordillera, Southern Spain), where the benthic foraminiferal turnover and extinction event associated with the negative carbon isotope excursion (CIE) across the PETM have been investigated. Detailed quantitative analyses of benthic foraminifera allowed us to distinguish assemblages with paleoecological and paleoenvironmental significance: pre-extinction fauna, extinction fauna, survival fauna (including disaster and opportunistic fauna) and recovery fauna. These assemblages have been associated with significant parts of the $\delta^{13}C$ curve for which a relative chronology has been established. The correlation between the benthic turnover, the $\delta^{13}C$ curve, the calcite and silicate mineral content, and sedimentation rates, allowed us to establish the sequence of events across the PETM. At Alamedilla, the benthic extinction event (BEE) affected ~37% of the species and it has been recorded over a 30-cm-thick interval that was deposited in c.a. 10 ky, suggesting a gradual but rapid pattern of extinction. The beginning of the BEE coincides with the onset of the CIE (+0 ky) and with an interval with abundant calcite, and it has been recorded under oxic conditions at the seafloor (as inferred from the benthic foraminiferal assemblages and the reddish colour of the sediments). We conclude that dissolution and dysoxia were not the cause of the extinctions, which were probably related to intense warming that occurred before the onset of the CIE.

The BEE is immediately overlain by a survival interval dominated by agglutinated species (the *Glomospira* Acme). The low calcite content recorded within the survival interval may result from the interaction between dilution of the carbonate compounds by silicicate minerals (as inferred from the increased sedimentation rates), and the effects of carbonate dissolution triggered by the shoaling of the CCD. We suggest that *Glomospira* species (disaster fauna) may have bloomed opportunistically in areas with methane dissociation, in and around the North Atlantic. The disaster fauna was rapidly replaced by opportunistic taxa, which point to oxic and, possibly, oligotrophic conditions at the seafloor. The CCD gradually dropped during this interval, and calcite preservation improved towards the recovery interval, during which the $\delta^{13}C$ values and the calcite content recovered (c.a. +71.25 to 94.23 ky) and stabilized (>94.23 ky), coeval with a sharp decrease in sedimentation rates.

1. Introduction

The generally warm, greenhouse world of the Paleogene underwent significant disruption at the Paleocene–Eocene transition, c.a. 55 Ma ago, when temperatures increased by 5° to 9 °C in the oceans and on land within less than 10,000 years (e.g., Röhl et al., 2000; Thomas, 2007). A major perturbation of the global carbon cycle occurred during this episode that is commonly known as the Paleocene–Eocene Thermal Maximum (PETM; Zachos et al., 1993), including a negative 2.5 to 6‰ carbon isotope excursion (CIE) in marine and terrestrial $\delta^{13}C$ values of carbonate and organic carbon (e.g., Kennett and Stott, 1991; Thomas and Shackleton, 1996; Zachos et al., 2001; Bowen et al., 2006) and a ~2 km shoaling of the calcite compensation depth (CCD) in the deep-sea (e.g., Zachos et al., 2005). The onset of these anomalies occurred during a time period <20 ky (Röhl et al., 2000, 2007), whereas subsequent recovery of $\delta^{13}C$ values took 170 ky (Röhl et al., 2007). This global perturbation of the carbon cycle is interpreted in terms of a rapid input of isotopically light carbon into the ocean–atmosphere system, possibly related to the massive dissociation of marine methane hydrates, although the triggering mechanism is still under debate (e.g., Dickens et al., 1997; Katz et al., 2001; Cramer and Kent, 2005; Pagani et al., 2006; Sluijs et al., 2007a).

Rapid changes in terrestrial and marine biota occurred during the PETM, including the most severe extinction of deep-sea benthic foraminifera recorded during the Cenozoic (e.g., Tjalsma and Lohmann,

* Corresponding author. Fax: +34 976 761106.
E-mail address: laia@unizar.es (L. Alegret).

0031-0182/$ – see front matter © 2009 Elsevier B.V. All rights reserved.
doi:10.1016/j.palaeo.2009.05.009

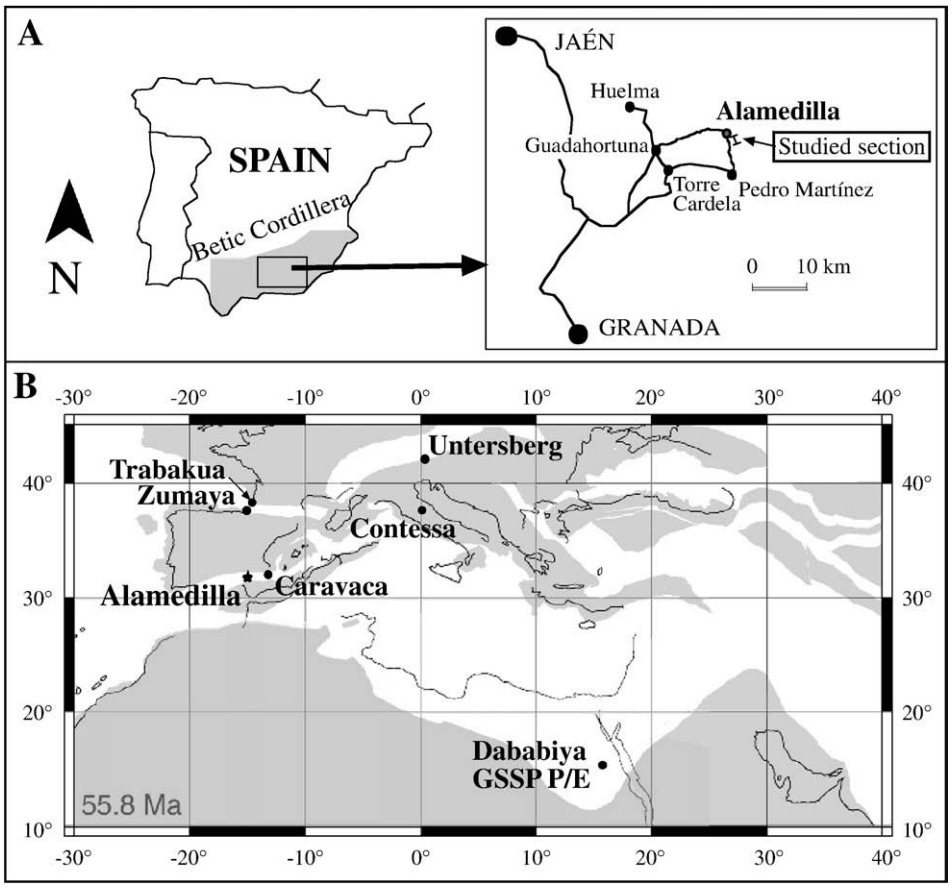

Fig. 1. A) Location of the Alamedilla section, and other Paleocene–Eocene sections referred to in the text. B) Paleogeographical reconstruction modified from Hay et al. (1999). GSSP = Global Stratotype Section and Point.

1983; Thomas, 2007), a global acme of the dinoflagellate genus *Apectodinium* and its migration to high latitudes (e.g., Crouch et al., 2001; Sluijs et al., 2007a,b), an acme of the planktic foraminiferal genus *Acarinina* and its migration towards higher latitudes (e.g., Arenillas and Molina, 1996; Kelly et al., 1998; Molina et al., 1999), the rapid evolutionary turnover of calcareous nannoplankton (e.g., Bralower, 2002; Stoll, 2005), the extinction and origination of shallow-water larger benthic foraminifera (e.g., Pujalte et al., 2003), latitudinal migration of plants (Wing et al., 2005) and a rapid radiation of mammals on land (e.g., Koch et al., 1992). The relation between carbon cycle perturbation, global warming and coeval biotic changes is not completely understood, because of the different response that individual ecosystems may have had to the effects of carbon release (Bowen et al., 2006). In particular, the causes of the rapid (<10 ky) benthic extinction event (BEE) in the deep-sea are not yet clear (e.g., Thomas, 2007). Many deep-sea species that had survived the global environmental crisis of the Cretaceous/Paleogene boundary (e.g., Alegret and Thomas, 2005, 2007; Alegret, 2007) went extinct at the PETM, and were replaced by post-extinction faunas of paleogeographically varying taxonomical composition (e.g., Thomas, 1998). In addition, in many sites and sections (including the Tethys area) the BEE coincides with carbonate-depleted intervals that are almost barren of calcareous foraminifera (Ortiz, 1995; Thomas, 1998; Alegret et al., 2005, 2009). Whereas several studies on deep-sea benthic foraminifera from the central Tethys have been recently carried out (e.g., Galeotti et al., 2004; Giusberti et al., 2007, 2009), published data from the western Tethys have only been reported from the Caravaca section in Southern Spain (Ortiz, 1995), where the benthic foraminiferal record of the basal CIE is strongly affected by dissolution. In contrast, a continuous succession of upper Paleocene and lower Eocene sediments is very well exposed at Alamedilla (33°N, Southern Spain; e.g., Arenillas and Molina, 1996; Lu et al., 1996; Monechi et al., 2000). We document in detail the benthic foraminiferal turnover and extinction event associated with the carbon isotope excursion (CIE) at Alamedilla. In order to infer paleoenvironmental consequences of the PETM, the benthic foraminiferal results have been integrated with geochemical and mineralogical data (Lu et al., 1996, 1998); the recognition of several benthic foraminiferal assemblages within distinct portions of the $\delta^{13}C$ curve may be a useful tool for correlation and paleoenvironmental reconstruction across the Paleocene–Eocene warming event.

2. Materials and methods

A continuous succession of upper Paleocene and lower Eocene pelagic sediments is very well exposed at Alamedilla (Southern Spain; Fig. 1), in the central Subbetic Cordillera (e.g., Arenillas and Molina, 1996; Monechi et al., 2000).

Upper Paleocene sediments consist of gray marls, with a 15-cm-thick turbiditic layer intercalated in the lower part of the studied section. The onset of the carbon isotope excursion (CIE) was identified by Lu et al. (1996, 1998) in sample 13.25, in a level of pink marls that grade into a 30-cm-thick red clay interval (meters 13.50 to 13.80; Fig. 2). These authors used X-ray diffraction to determine the mineral composition of bulk sediment, and distinguished calcite, detritus (defined as quartz, K-feldspar and plagioclase) and phyllosilicates (wt.%). In coincidence with the onset of the CIE, these authors documented a decrease in the percentage of calcite and an increase in the percentage of silicate minerals, which make up to 12% of the whole rock composition during the core of the CIE. However, due to the low sampling resolution in the lowermost Eocene in the study by Lu et al. (1996), we carried out analyses of the $\%CaCO_3$ in some samples across the critical BEE interval (Figs. 2, 5). The red clay

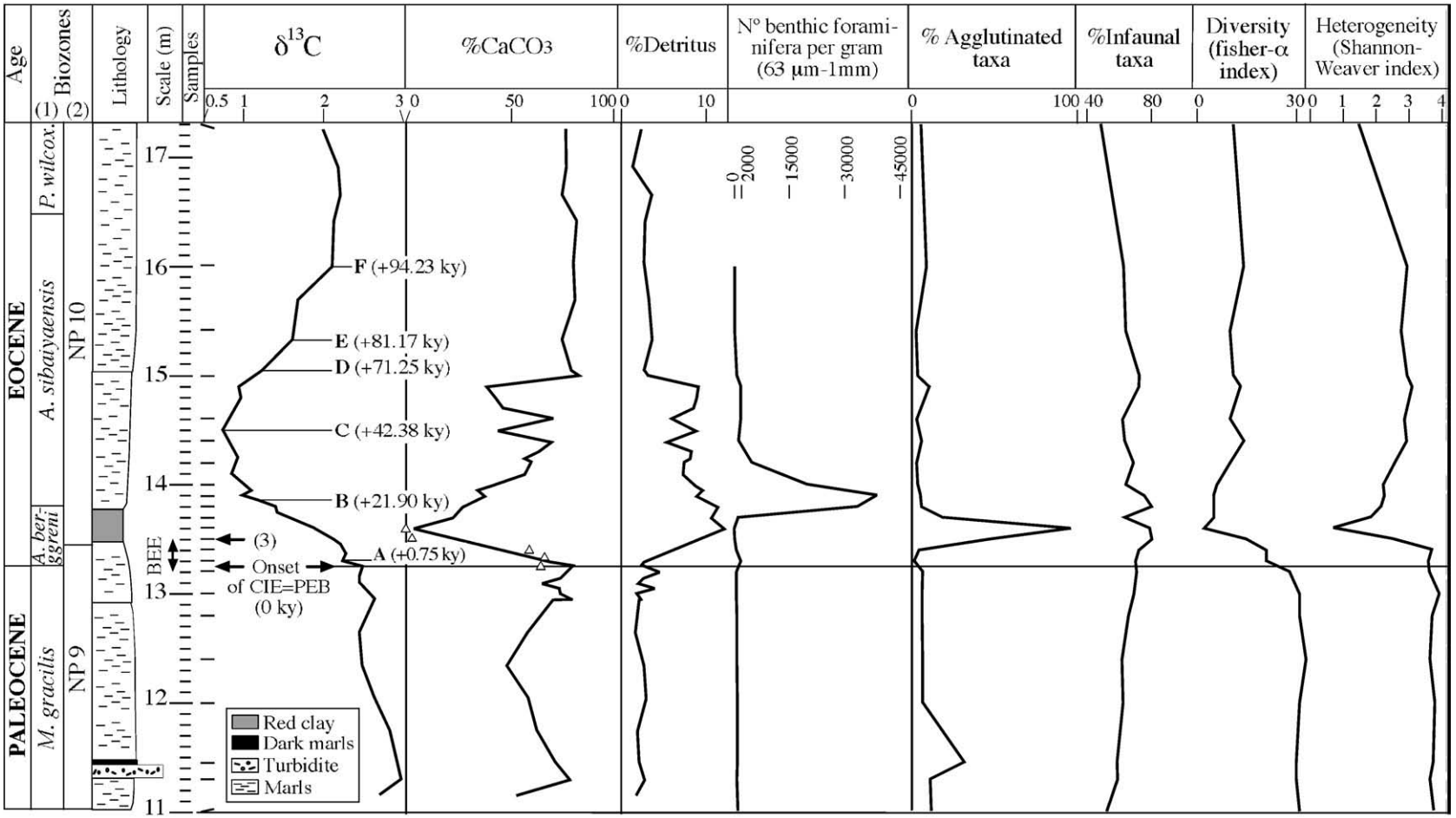

Fig. 2. $\delta^{13}C$ curve (in bulk sediment) and percentages of $CaCO_3$ and detritus (silicate minerals) at Alamedilla (modified from Lu et al., 1996). Age model (A–F) according to Röhl et al. (2007). Number of benthic foraminifera per gram of washed residue 63 μm–1 mm, percentages of agglutinated and infaunal taxa, and diversity and heterogeneity indices across the upper Paleocene and lower Eocene. White triangles represent the $\%CaCO_3$ analyses carried out across the critical BEE interval in this study. (1) Arenillas and Molina (1996) and Molina et al. (1999); (2) Monechi et al. (2000). *M.* = *Morozovella; A.* = *Acarinina; P. wilcox.* = *Pseudohastigerina wilcoxensis;* (3) Highest occurrence of *Stensioeina beccariiformis*. CIE = Carbon Isotope Excursion. PEB = Paleocene/Eocene boundary.

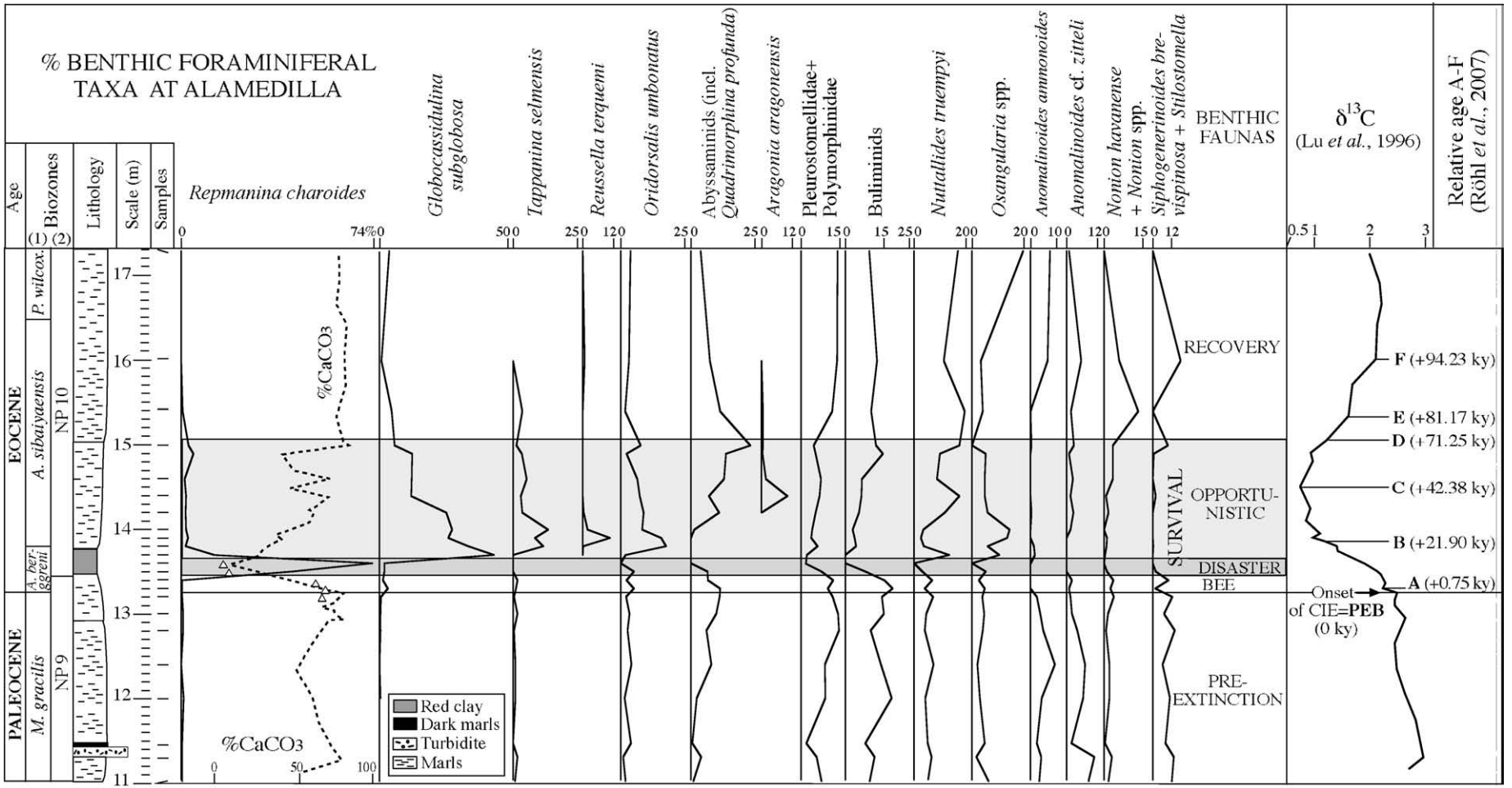

Fig. 3. Stratigraphic distribution and relative abundance of benthic foraminiferal taxa across the upper Paleocene and lower Eocene at Alamedilla. Note that species that disappear in the Paleocene–Eocene transition have been represented in Fig. 4. $\delta^{13}C$ curve (in bulk sediment) and percentages of calcite modified from Lu et al. (1996). White triangles represent the $\%CaCO_3$ analyses carried out across the critical BEE interval in this study. (1) Arenillas and Molina (1996) and Molina et al. (1999); (2) Monechi et al. (2000). *M.* = *Morozovella; A.* = *Acarinina; P. wilcox.* = *Pseudohastigerina wilcoxensis.*

interval is overlain by red marls and, higher up in the section, by gray marls (Fig. 2).

In addition to geochemical and mineralogical studies (Lu et al., 1996, 1998), the planktic foraminiferal and nannofossil faunal turnover across the PETM at Alamedilla have been documented (Arenillas and Molina, 1996; Lu et al., 1996; Monechi et al., 2000), but benthic foraminifera have not been studied in detail, so far. A total of 24 samples have been studied across the studied interval, encompassing the uppermost 2.25 m of the Paleocene and the lowermost 4 m of the Eocene. Samples were picked at 10 to 20 cm intervals across the onset and in the "core" of the CIE, and at ~40 cm intervals below and above it (Fig. 2). The position of the studied samples was correlated to the results by Lu et al. (1996, 1998). Preservation of benthic foraminiferal tests is moderate across the studied section, although the preservation of calcareous tests is poor in the lowermost Eocene, improving upsection.

Quantitative studies of benthic foraminifera were based on representative splits (using a modified Otto micro-splitter) of approximately 300 specimens larger than 63 μm (Plate I). The number of benthic foraminifera per gram of residue (63 μm–1 mm), the percentages of benthic foraminiferal taxa (Fig. 3), the calcareous/agglutinated ratio, and several proxies for benthic foraminiferal diversity (Fig. 2) such as the Fisher-a index and the H(S) Shannon–Weaver information function (Murray, 1991) were calculated. Probable microhabitat preferences and environmental parameters were inferred from the benthic foraminiferal morphotype analysis (e.g., Corliss, 1985, 1991; Jones and Charnock, 1985; Corliss and Chen, 1988; Jorissen et al., 1995). Paleobathymetrical inferences were based on benthic foraminiferal data, especially on the occurrence and abundance of depth-related species, their upper depth limits, and through the comparison between fossil and recent assemblages (e.g., Van Morkhoven et al., 1986; Alegret et al., 2001, 2003). We followed the bathymetric division defined in Van Morkhoven et al. (1986): upper bathyal = 200–600 m, middle bathyal = 600–1000 m, lower bathyal = 1000–2000 m and abyssal >2000 m.

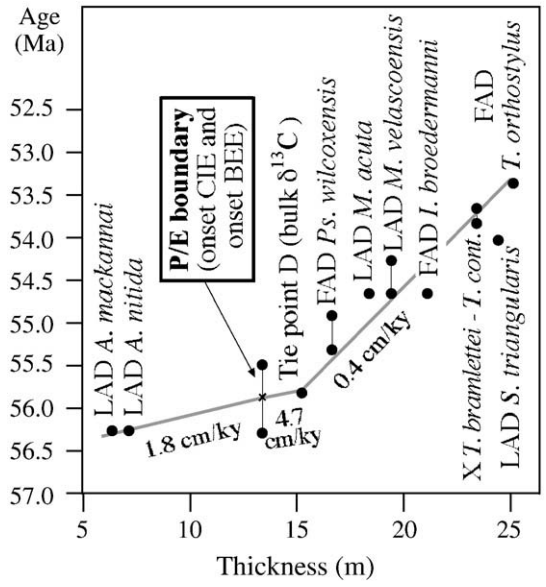

Fig. 4. New age model and sedimentation rates for the sections below and above the CIE at Alamedilla, mainly based on depths of datum levels of planktic foraminifera (Arenillas and Molina, 1996), and calcareous nannofossils (Monechi et al., 2000), and on numerical ages according to the timescales applied to ODP Leg 208 (Shipboard Scientific Party, 2004) and in Berggren and Pearson (2005). LAD: Last Appearance Datum; FAD: First Appearance Datum; X: Abundance crossover. Age of the P/E boundary according to Westerhold et al. (2008). *A.* = *Acarinina; I.* = *Igorina; M.* = *Morozovella; Ps.* = *Pseudohastigerina; S.* = *Subbotina; T.* = *Tribrachiatus; T. cont.* = *T. contortus*. A 1.8 cm/ky and 0.4 cm/ky sedimentation rate has been inferred for the uppermost Paleocene and lower Eocene, respectively, compared to the 2.4 cm/ky and 0.7 cm/ky inferred by Lu et al. (1996). These results are somewhat different, but in the same order of magnitude. Note the increase in sedimentation rates (4.7 cm/ky) at the P/E boundary (13.25 m), through the interval with a high percentage of silicate minerals (15 m). From that level upwards, sedimentation rates remain low (0.4 cm/ky) for the rest of the studied interval.

For biostratigraphical control, we follow the planktic foraminiferal and calcareous nannofossil zones identified by Arenillas and Molina (1996), Molina et al. (1999) and Monechi et al. (2000) at Alamedilla (Figs. 2, 3). In order to infer the timing across the CIE interval at Alamedilla, we studied the shape of the bulk carbonate $\delta^{13}C$ curve at Alamedilla and compared it to the bulk carbonate $\delta^{13}C$ curve from Ocean Drilling Program Site (ODP) 690, for which a high-resolution age model has been recently developed by Röhl et al. (2007). The main peaks and plateaus of this curve may be related to the rapid changes in the input and removal of isotopically light carbon across the PETM (e.g., Röhl et al., 2000). Based on this idea, we followed the orbitally calibrated timescale by Röhl et al. (2007) and chose six tie points (A–F; Fig. 2): Paleocene/Eocene boundary (PEB) = 0 ky, A = 0.75 kr, B = 21.90 ky, C = 42.38 ky, D = 71.25 ky, E = 81.17 ky, F = 94.23 ky. The correlation between the CIE at Alamedilla and ODP Site 690 is problematic because the onset of the excursion appears to be less abrupt at Alamedilla. This might result from a lower time resolution of the bulk carbonate record in Lu et al. (1996) than in the Bains et al. (1999) record for Site 690. Provided the small initial shift in bulk $\delta^{13}C$ at Alamedilla is indeed coeval with the larger initial shift at Site 690, one could argue that the record is much more complete at Alamedilla, at least over the beginning of the CIE, making it one of the most complete marine records over that interval.

In addition, we show a new age model and sedimentation rates for the sections below and above the CIE at Alamedilla (Fig. 4), based on depths of datum levels and numerical ages according to the timescales applied to ODP Leg 208 (Shipboard Scientific Party, 2004). This new age model updates that proposed by Lu et al. (1996) for Alamedilla.

3. Faunal turnover

Quantitative results of the benthic foraminiferal analyses are shown in Figs. 2 and 3, and in Table 1. Benthic foraminiferal assemblages are strongly dominated by calcareous taxa (~90% of the assemblages) in all samples but two (13.50 and 13.60), where agglutinated taxa make up 47% and 96% of the assemblages, respectively. Infaunal morphogroups are dominant through the whole studied interval, making up 52–79% of the assemblages. The following benthic foraminiferal assemblages have been recognised across the Paleocene–Eocene transition at Alamedilla.

3.1. Pre-extinction fauna

Assemblages just below the extinction event (samples 11 to 13.20) are diverse (Fisher-α index ~31) and heterogeneous (Shannon–Weaver index ~3.7; Fig. 2), and dominated by buliminids (*Bolivinoides delicatulus*, *Bulimina kugleri*, *Bulimina trinitatensis*), polymorphinids, *Anomalinoides* spp. (*A. ammonoides, A.* cf. *zitteli*), *Cibicidoides hyphalus*, *C. pseudoperlucidus*, *Nuttallides truempyi*, *Osangularia*, *Stensioeina beccariiformis*, *Siphogenerinoides brevispinosa*, *Stilostomella* spp., etc. (Fig. 3). The composition of the assemblages is slightly different (higher percentages of agglutinated taxa such as *Clavulinoides amorpha* and *Gaudryina pyramidata*) in sample 11.45, which is associated to a ~15-cm-thick turbidite deposited 2 m below the P/E boundary.

The relative abundance of infaunal morphogroups increases from the bottom of the section (52%) towards the horizon of the main BEE (sample 13.50), where they show maximum values (79% of the assemblages). Diversity decreases, and the percentage of *Abyssamina quadrata* starts to increase (making up to 10% of the assemblages) ~20–25 cm below the onset of the CIE, coeval with a decrease in the relative abundance of *Anomalinoides* spp.

3.2. The benthic foraminiferal extinction event

The highest occurrences of 32 benthic foraminiferal species are recorded in the uppermost Paleocene at Alamedilla, 6 of which correspond

Table 1
Benthic foraminiferal counts for the upper Paleocene and lower Eocene samples from Alamedilla.

Benthic foraminiferal taxa	Samples (m)																							
	Al-11	Al-11,30	Al-11,45	Al-12	Al-12,40	Al-12,80	Al-13	Al-13,20	Al-13,30	Al-13,40	Al-13,50	Al-13,60	Al-13,70	Al-13,80	Al-13,90	Al-14	Al-14,20	Al-14,40	Al-14,60	Al-14,90	Al-15	Al-15,40	Al-16	Al-17,30
Abyssamina quadrata		3		5	5	9	23	33	23	16	8							4	9	11	33	6	6	
Abyssamina sp.			1		1	6	5	1													20			1
Alabamina sp.	5	4	1		3	3	1	2		2	1								1		3			3
Allomorphina sp.										1														
Allomorphina trochoides				2	3	4	3	5		4													1	
Angulogavelinella avnimelechi	2		1			1	1																	
Angulogerina sp.				1				1																
Anomalinoides affinis									1															
Anomalinoides ammonoides	10	12	7	13	22	14	11	8					5	6			1				1		8	8
Anomalinoides cf. *praeacutus*																		1						
Anomalinoides cf. *zitteli*	25	32	6	19	17	12	6	5	3	7						5	8	4	6	3	9	3	7	1
Anomalinoides rubiginosus	1	1	7																					
Anomalinoides spp.	6	11	6	15	1	5	10	3	26	26	7		6	23	20	44	23	13	40	25	16	11		2
Aragonia aragonensis																		27	4	1	2	1		
Aragonia velascoensis			3				1	4																
Arenobulimina truncata	3		1					3		2														
Astacolus spp.	1		1				2		2	1														
Bathysiphon spp.				2				2					1					3				2	6	
Bolivinoides delicatulus	2	1	2	7	1	2	5	12	1	1														
Bolivinoides spp.			1	7	7											1		9						
Brizalina spp.									4	3								1	1					
Bulimina alazanensis							1																	
Bulimina kugleri	4	8	3	8	6	6	6	5	24	22	6					1				1		7		4
Bulimina midwayensis															1			1		1				
Bulimina sp. 1	2	6	1	4	2	6	2	2		2						4			3	4	8	4		
Bulimina spp.	5	6	3	8	6	4	3	8	4	4	3			1	2		2	1		13	7		8	1
Bulimina trinitatensis	3	1	5	3	1	6	3	5	1											5		4	2	
Bulimina tuxpamensis		2	1				8		3	3				20	5		9	4	10	13	16		3	4
Bulimina velascoensis					3			1	3															
Buliminella beaumonti	1	1	4	3			1	4	1	1	1					3	5	1	2	5	3		2	
Buliminella grata		1	3				3		2	1														
Buliminella sp.					1										3						4			1
Cibicidoides cf. *howelli*	2		3	4	2		2		1	1	1													
Cibicidoides dayi									1	1														
Cibicidoides eocaenus			1				1	1																
Cibicidoides hyphalus	11	2	8	5			2	5	4	1														
Cibicidoides proprius										1														
Cibicidoides pseudoperlucidus	4	3	12			1	5			1				1			1	6	3	3	1		1	
Cibicidoides spp.	1	2	1	1	1	4			5	10			2	3			2	3	3	1				
Cibicidoides velascoensis			2			1	1		2															
Cibicidoides westi				2				1	2								1	2				1		
Clavulinoides amorpha	2	3	17	1																				
Clavulinoides spp.						1				1														5
Clavulinoides trilatera			1	1																				
Coryphostoma midwayensis	6	4		7	2	2	9	5	3	5														
Coryphostoma spp.	1			1	3	1			4											1	1			
Dorothia crassa		1				2	2																	
Dorothia cylindracea	1				2		5																	
Dorothia pupa			1				1			1														
Dorothia sp.						1				3														1
Ellipsoglandulina spp.			1	2			1		3	3	1		5						1	1				

(continued on next page)

Table 1 (*continued*)

Benthic foraminiferal taxa	Samples (m)																							
	Al-11	Al-11,30	Al-11,45	Al-12	Al-12,40	Al-12,80	Al-13	Al-13,20	Al-13,30	Al-13,40	Al-13,50	Al-13,60	Al-13,70	Al-13,80	Al-13,90	Al-14	Al-14,20	Al-14,40	Al-14,60	Al-14,90	Al-15	Al-15,40	Al-16	Al-17,30
Ellipsopolymorphina sp.										3	1								1	1				
Eouvigerina sp.					1	1			1	9										2				
Fissurina sp.	2	6			1	5				1	3						1							
Fursenkoina spp.									4	8										1		2		
Gaudryina pyramidata	3	2	8		3			3																
Gaudryina sp. 1		2	3	2		1																		
Gaudryina sp. *Juvenile*	7	4	19			1	4	5		1														
Gaudryina spp.	1		5																					
Gaudryina spp. *indet*			15																					
Glandulina spp.							3		1	1							3						5	1
Globocassidulina subglobosa						1	1	2	11	5	3	1	140	167	81	87	78	33	31	38	19	8	1	4
Globorotalites sp.									3		1													
Globulina spp.	2	1		4	3	5	7		5	3	1				1									
Guttulina spp.					1	1				1										1				
Gyroidinoides beisseli	2	3		2	2	4		2	1	1							1							
Gyroidinoides depressus				2	1	1			1		1					1								
Gyroidinoides girardanus	1	1	2		1		3	2	3															
Gyroidinoides globosus	1	2		3	4	1		7		1														
Gyroidinoides spp.	6	4	3	1	2		4	1					2								1			
Gyroidinoides subangulatus	1			2		1	1	1		1														
Hemirobulina spp.		3		9	2		3																	
Hyperammina sp.			1																					
Karrerulina sp.	2			3			1			1								1		3				
Laevidentalina spp.	5	7		4	8	8		5	23	18	2		2	4	2	2	3	6	7	10	4	3		
Lagena spp.	6	4		10	4	8	4		5	11	1						1	3	2		1	3		4
Lenticulina spp.	3	5	7	2	4	5	8	11	6	8					1			1		1	2	3		3
Marssonella oxycona	1	1	1																					
Marssonella sp. *Juvenile*		1	2			1		1		1														
Miliolids																	1							
Neoflabellina jarvisi			1	2		1																		
Nonion havanense	2	8	1	1	1	1	1	4	8	12	1		1	4	3		5	2	4	10	7	22	6	
Nonion spp.	3	2		5	4	1	3	8											4		4		1	
Nonionella cf. *cretacea*										1														
Nonionella sp.	11	16	1	12	8	12	5	5	7											5	5		2	
Nuttallides truempyi	16	20	16	13	18	12	14	24	14	24	5		43	18	8	11	36	47	22	30	57	33	14	18
Nuttallinella florealis	1	2	2	1	1	5	5	3	2	3	1													
Nuttallinella sp.									5				4						3					
Oridorsalis sp.													2											
Oridorsalis umbonatus	6	3	12	5	10	8	10	7	17	8	8		6	86	48	26	27	20	16	7	25	3	4	4
Osangularia spp.	18	5	10	9	5	12	12	13	16	9	5		33	29	41	45	18	13	12	16		7	4	21
Osangularia velascoensis	1		5				2			1	3													
Paralabamina hillebrandti	10	6	10	6	2	14	3	6	4	1				1		1	1					2		2
Pleurostomella sp.	3	3		6	2	4	5	5	9	10	1		1	19	11	13	14	15	15	12	11	14	9	2
Polymorphinids	13	10	4	8	14	27	26	35	15	21	3		1	12			3	3		2	5	6	8	13
Praebulimina sp.									2															
Pseudoclavulina trinitatensis	1		2																					
Pseudouvigerina sp.																	1							
Pullenia coryeli	3	2	1	1	1	2	1	5		3	1													
Pullenia cretacea	3		12		1					3														
Pullenia quinqueloba	1							2																
Pullenia sp.			1	1			4											1					1	
Pyramidina rudita	3	4				2	1	3	1	2														
Pyrulinoides spp.	5	4	1	8	2	6	3		2	2	5	1						1	2					

Quadratobuliminella pyramidalis	1		1	6	1		2	2	4	1	2													
Quadrimorphina allomorphinoides																		1		1				
Quadrimorphina profunda	3	9	1	2	13	3	1	3	15	7	2					4	33	15	23	30	22	13	3	3
Ramulina sp.									1															
Recurvoides spp.																1								
Remesella varians			1		1	1		4																
Repmanina charoides	1	1	1	3		2	2	1	1	1	66	40	40	8	8	6	5	5	3	14	9	1		
Reussella terquemi														1	32	6	1						1	
Rzehakina sp.	1																							
Rhabdammina sp.																		1						
Rhizammina spp.									1		1					1	1		2	1				
Saracenaria spp.						2		1													1			
Siphogenerinoides brevispinosa	4	9	2	4	1	4		5	3	11											2			
Spiroplectammina navarroana																				6				
Spiroplectammina sp.					1				1											1				
Spiroplectammina spectabilis	3	6	8	4	2		2		2	3														
Stensioeina beccariiformis	9	3	16	8	5	6	7	12	7	8	1													
Stilostomella spp.	19	15	13	16	8	21	13	20	2	10	2			1				3		1	17		13	
Tappanina selmensis	2	5		3	2	1	5	1	4	6				57	26	42	11	8	13	10	4	6		
Trochamminids	9	13	7	9	7	9	2	3		2	5	12	20	22	9	4	4	6	3	7	3	2	5	
Uvigerina sp.									1									1						
Vulvulina sp.			3																					
Total	293	296	302	298	236	291	292	328	331	347	153	54	314	483	302	308	300	266	246	298	323	167	121	106

to local disappearances and 26 to real extinctions (e.g., *Angulogavelinella avnimelechi*, *Anomalinoides rubiginosus*, *Arenobulimina truncata*, *Bolivinoides delicatulus*, *Cibicidoides hyphalus*, *C. howelli*, *C. velascoensis*, *Coryphostoma midwayensis*, *Dorothia pupa*, *Gyroidinoides subangulatus*, *Marssonella oxycona*, *Neoflabellina jarvisi*, *Nuttallinella florealis*, *Osangularia velascoensis*, *Pullenia coryelli*, *Stensioeina beccariiformis*; Fig. 5). These and other species have been documented to become extinct globally (e.g., Tjalsma and Lohmann, 1983; Van Morkhoven et al., 1986; Thomas, 1990, 1998; Bolli et al., 1994; Kaminski and Gradstein, 2005).

The onset of the extinctions coincides with the onset of the CIE (sample 13.25, Lu et al., 1996), and only one species (*Clavulinoides amorpha*) last occurs below it. The extinction event has been identified over a 30-cm-thick interval and it affected ~37% of the species, with the last appearances recorded in samples 13.20, 13.30, 13.40 and 13.50 (lowermost Eocene; Fig. 5). The whole residue of the samples studied within this interval was searched for the extinction taxa in order to minimize the Signor–Lipps effect.

Since the analyses of the calcite content carried out by Lu et al. (1996) were at a lower resolution than our samples, we analysed the percentage of calcite in critical samples across the BEE (Fig. 5). Our results show percentages of calcite higher than 55% in the first three samples of the BEE interval (13.20, 13.30 and 13.40), whereas these values drop to almost 0 in samples 13.50 and 13.60. These results indicate that the beginning of the extinctions is recorded over an interval with high levels of calcite (samples 13.20 to 13.40).

3.3. Survival interval

3.3.1. The disaster fauna

Disaster species are taxa specifically adapted to stressed environmental conditions associated with mass extinction intervals, who develop short-lived, relatively large populations ("blooms") immediately following crises, early in the survival phase, within a thin stratigraphical interval containing rare fossils (Kauffman and Harries, 1996; Kauffman et al., 1996).

At Alamedilla, after the BEE, diversity and heterogeneity of the assemblages reached the lowest values in the section (Fisher-α index = 4 and Shannon–Weaver index = 0.7 in sample 13.60; Fig. 2). The high dominance of the assemblages is related to the occurrence of a disaster fauna (samples 13.50 to 13.60), which dramatically increased in relative abundance after the extinction event at Alamedilla. This fauna is strongly dominated by *Repmanina* (*Glomospira*) *charoides* and *Glomospira* spp., and it corresponds to the commonly called early Eocene "*Glomospira* Acme", which may be useful for stratigraphic correlation across the *P–E* transition in deep-water settings of western Tethys and North Atlantic (e.g., Kaminski and Gradstein, 2005).

The disaster fauna has been identified in two consecutive samples (13.50 and 13.60) that contain the lowest calcite content and a decrease in bulk carbonate δ^{13}C values (Figs. 2, 5). The percentage of silicate minerals increases in these samples (up to 12%), and remains high (~9%) for the rest of the CIE, until sample 14.90 (Fig. 2).

3.3.2. Opportunistic fauna

The population increase in disaster taxa is extremely short-lived, as they are quickly replaced by opportunists and other survivors early in the repopulation phase; opportunistic taxa are capable of prolific population expansion and rapid biogeographical dispersal into stressed environments (Kauffman and Harries, 1996; Kauffman et al., 1996).

An opportunistic fauna dominated by calcareous taxa (samples 13.70 to 15) has been identified just 10 cm above the interval characterised by the disaster fauna. Several peaks in the abundance of opportunistic taxa have been recorded coinciding with a gradual increase in diversity and heterogeneity of the assemblages (Fig. 2). A bloom in *Globocassidulina subglobosa* (which makes up to 45% of the assemblages), increased percentages of *Nuttallides truempyi* and *Osangularia* spp., and a dramatic increase in the absolute abundance of benthic foraminifera (nr/gr 63 μm–1 mm) are recorded at the beginning of this interval (Fig. 3). These are followed by a short-lived increase in the relative abundance of *Tappanina selmensis*, *Oridorsalis umbonatus* and *Reussella terquemi* (samples 13.80 to 14; Fig. 3). Note that these peaks, combined with the increase in absolute abundance of benthic foraminifera, mean that these species strongly increased in numbers.

A rapid decrease in the absolute abundance of benthic foraminifera in sample 14.20 is followed by a peak in relative abundance of *Aragonia aragonensis*, increased percentages of *Abyssamina quadrata* and *Quadrimorphina profunda*, minimum values in the bulk carbonate δ^{13}C record, and strong fluctuations in the calcite content (Figs. 2, 3).

The percentage of buliminids gradually increases through this interval (up to 15% of the assemblages), but they do not reach the pre-extinction values.

3.4. Recovery fauna

During the recovery and stabilization of the bulk carbonate δ^{13}C values, increase in $CaCO_3$ content and decrease in the percentage of silicate minerals to pre-extinction values (Fig. 2), a recovery fauna dominated by trochospiral morphotypes (abundant *Nuttallides truempyi* and *Osangularia* spp., and common *Anomalinoides* spp.) and cylindrical tapered morphotypes (e.g., buliminids, *Pleurostomella* spp., *Stilostomella* spp.) has been observed at Alamedilla (samples 15.40 to 17.30; Fig. 3). The percentage of cylindrical tapered taxa increases up to pre-extinction values. The relative abundance of abyssaminid species and *Nonion havanense* decreases across this interval, whereas the percentage of *Osangularia* increases (Fig. 3). Diversity and heterogeneity of the assemblages do not reach the pre-extinction values.

4. Discussion

The stratigraphic distribution of calcareous and agglutinated benthic foraminiferal species, and the composition of their assemblages at Alamedilla are similar to those of other deep-water (lower bathyal to abyssal) sections in the western Tethys, such as Zumaia and Trabakua Pass sections in northern Spain (Orúe-Etxebarria et al., 1996; Alegret et al., 2009), Untersberg section in Austria (Egger et al., 2005) or Contessa section in Italy (Galeotti et al., 2004; Giusberti et al., 2009). Within the CIE interval the agglutinated assemblage is dominated by *Glomospira* spp. in all these sections but Zumaia, and the post-extinction calcareous benthic foraminiferal assemblages are dominated by *Nuttallides truempyi*, abyssaminids, buliminids, *Anomalinoides* spp., *Oridorsalis* (including *O. umbonatus*) and various pleurostomellids.

4.1. The uppermost Paleocene

Benthic foraminiferal assemblages are diverse and contain abundant Paleocene cosmopolitan species (e.g., Tjalsma and Lohmann, 1983; Van Morkhoven et al., 1986). Representatives of the bathyal and abyssal Velasco-type fauna (Berggren and Aubert, 1975), such as *Aragonia velascoensis*, *Cibicidoides velascoensis*, *Gyroidinoides globosus*, *Nuttallides truempyi*, *Nuttallinella florealis*, *Osangularia velascoensis* and *Stensioeina beccariiformis*, are common at Alamedilla. Assemblages are dominated by species that have an upper depth limit at lower bathyal depths, namely *Bulimina trinitatensis*, *B. tuxpamensis*, *Buliminella grata*, *Nuttallides truempyi* and *Stensioeina beccariiformis* (e.g., Van Morkhoven et al., 1986; Alegret et al., 2003). High percentages of *Abyssamina quadrata* and *Quadrimorphina profunda*, which are most common at abyssal depths (Tjalsma and Lohmann, 1983), have been recorded. These data indicate a lower bathyal–upper abyssal depth of deposition during the late Paleocene at Alamedilla.

The calcareous-dominated assemblages from the upper Paleocene indicate deposition above the CCD. The diversity of the assemblages,

and the occurrence of abundant taxa with large and heavily calcified tests, indicate well-oxygenated bottom waters during the late Paleocene. The gradual increase in infaunal morphogroups towards the uppermost Paleocene may point to a slight increase in the food supply to the seafloor.

4.2. The core of the CIE

4.2.1. The onset of the CIE and the benthic foraminiferal extinction event

The BEE includes the extinction of ~37% of the species over a 30-cm-thick interval (in which 4 samples where analysed) at Alamedilla, and its onset has been recorded in coincidence with the onset of the CIE, as in Zumaia section (Alegret et al., 2009). Considering the relative ages of tie points A and B of the bulk carbonate $\delta^{13}C$ curve (Röhl et al., 2007), it may be inferred that the BEE was gradual but rapid, with a duration c.a. 10 kyr (from sample 13.20 to sample 13.50).

The BEE affected both calcareous and agglutinated foraminifera, and it is recorded across an interval (13.20 to 13.50) without strong evidence for bioturbation, and with a high calcite content in all samples but the uppermost one (13.50). This suggests that calcite dissolution was not the main cause of the extinctions, which started earlier (Fig. 5). Similarly, dysoxia was not the main cause of the BEE, since the faunal composition and the reddish colour of the marls and clays across the BEE interval indicate oxic conditions at the seafloor. Dysoxic or even anoxic conditions at the seafloor may have caused some extinctions locally, but not globally (e.g., Thomas, 2007).

Food is a limiting factor in the deep-sea, and small variations in the type or amount of nutrients may have dramatic consequences on the benthic assemblages. However, there is no agreement as to whether primary productivity in surface waters increased or decreased globally at the onset of the CIE (Bains et al., 2000; Bralower, 2002; Dickens et al., 2003; Tremolada and Bralower, 2004; Gibbs et al., 2006), whereas the extinction of deep-sea benthic foraminifera was global. Moreover, variations in surface primary productivity at Alamedilla are not clear (Monechi et al., 2000).

Food supply, oxygen conditions or dissolution seem not to be the cause of the extinctions at Alamedilla. Warming is likely to have been the only global feature of the PETM for which there was no refugia, triggering paleoecological and paleoenvironmental instability, and eventually leading to the gradual but rapid BEE. According to Thomas (2007), increased temperatures must have affected metabolic rates and, therefore, food cycling within ecosystems, although detailed isotope analyses are needed to determine whether warming occurred before or just at the beginning of the BEE. At Alamedilla, oxygen isotope analyses show a 4 °C warming in bottom waters at the Paleocene–Eocene transition (Lu et al., 1998).

4.2.2. The Glomospira Acme and the minimum calcite content

The *Glomospira* Acme has been identified at Alamedilla just above the BEE, in two samples (13.50 and 13.60) with a low calcite content and increased percentages of silicate minerals (Figs. 2, 3). The sharp increase in sedimentation rates (from 1.8 to 4.7 cm/ky; Fig. 4) in this interval points to dilution of the carbonate content by a high input of silicate minerals, although the lack of calcareous benthic foraminifera, and the poor preservation of the calcareous tests just above this level, suggests that carbonate dissolution may have affected the faunal composition. Widespread $CaCO_3$ dissolution has been documented from deep-sea settings, and related to the release of methane and increase in concentration of CO_2 during the PETM, which led to a drop in ocean pH and shoaling of the CCD (e.g., Dickens et al., 1997; Zachos et al., 2004; Zeebe and Zachos, 2007).

Recent species of *Glomospira* and *Repmanina* are mobile epifaunal forms that feed on organic detritus (e.g., Ly and Kuhnt, 1994), and tolerate large environmental fluctuations (e.g., Kaminski et al., 1996), whereas the oxygenation of bottom waters seems to be less important for this assemblage (Egger et al., 2005). In the Pliocene to modern Mediterranean, *R. charoides* displays the highest percentages in oligotrophic areas, responding more to changes in productivity rather than in oxygenation, and this acme has been related to unstable trophic conditions during the earliest Eocene (Kaminski and Gradstein, 2005). Given the fact that the *Glomospira* Acme is very widespread in western Tethys and northern Atlantic during the lowermost Eocene (e.g., Kaminski and Gradstein, 2005), we suggest that it may have bloomed opportunistically in areas with methane dissociation (which triggered increased chemosynthetic activity), as it does today in areas of active petroleum seepage in the Gulf of Mexico (Kaminski, 1988). Consequently, we suggest that the distribution of the *Glomospira* peaks might be related to areas with methane dissociation from gas hydrates (Katz et al., 1999, 2001) or from organic matter heated up by igneous intrusions (Svensen et al., 2004); both models locate the methane in the North Atlantic. Alternatively, *Glomospira* peaks might be common in regions associated with the volcanic ash deposits from the North Atlantic Volcanic Province (e.g., Egger et al., 2005).

4.2.3. The opportunistics

The disaster fauna was rapidly replaced by opportunistic taxa, which occur during intervals characterized by perturbed environmental conditions (Kauffman and Harries, 1996). These opportunistic species may have taken advantage of a high-stress, strongly fluctuating environment as a result of dramatic changes in oceanic ecosystems. Similar peaks in the relative abundance of opportunistic species have been observed across the PETM in other ODP and DSDP sites as well as in land sections (e.g., Thomas, 1998, 2003, 2007; Galeotti et al., 2004; Alegret et al., 2005, 2009), and their study may help to understand the long-term effects of the PETM. The benthic foraminiferal turnover across the PETM at Alamedillla is particularly similar to that recently reported from the Italian Contessa section (Giusberti et al., 2009), where the *Glomospira* Acme is followed by peaks in opportunistic taxa in the same stratigraphic order: *T. selmensis–O. umbonatus–A. aragonensis*-abyssaminids. However, the record at Contessa lacks the quantitative peak in *Globocassidulina subglobosa* that immediately overlies the *Glomospira* Acme at Alamedilla.

G. subglobosa is an oxic indicator in the modern oceans and its abundance has been related to a number of variables (e.g., Smart et al., 2007), although it is common with pulsed food inputs (e.g., Gupta and Thomas, 2003; Suhr et al., 2003; Suhr and Pond, 2006). The maximum abundance of *Tappanina selmensis* (tie point B, +21.90 ky; Röhl et al., 2007) in the interval with a low calcite content may indicate stressed sea floor conditions and bottom waters undersaturated in calcium carbonate (Boltovskoy et al., 1991; Takeda and Kaiho, 2007). A peak in relative abundance of *Aragonia aragonensis* is recorded in coincidence with minimum bulk carbonate $\delta^{13}C$ values (tie point C, +42.38 ky; Röhl et al., 2007). This species is common in post-extinction intervals at several ODP Sites (e.g., Thomas, 1998, 2003), and has been suggested to be an opportunistic species, as *T. selmensis* (Steineck and Thomas, 1996). Abyssaminid taxa (including *Abyssamina quadrata* and *Quadrimorphina profunda*) are small, thin-walled species that might indicate oligotrophy or might be opportunistic species (Takeda and Kaiho, 2007; Thomas, 2007). In addition to these peaks, the percentage of *Nuttallides truempyi* progressively increases towards the top of this interval. *N. truempyi* has been suggested to be a low-food indicator, although it might also be able to survive in carbonate corrosive waters, like its descendant *N. umbonifera* (Thomas, 1998), thus explaining its abundance next to samples with strong dissolution in the lowermost Eocene (e.g., Alegret et al., 2009).

We suggest that the benthic foraminiferal composition during the core of the CIE at Alamedilla points to oxic and, possibly, oligotrophic conditions at the seafloor. Even if the supply of organic particles remained constant, the high sedimentation rates (4.7 cm/ky; Fig. 4) during this interval would result in dilution of the organic compounds, and therefore, in more oligotrophic conditions at the seafloor. It

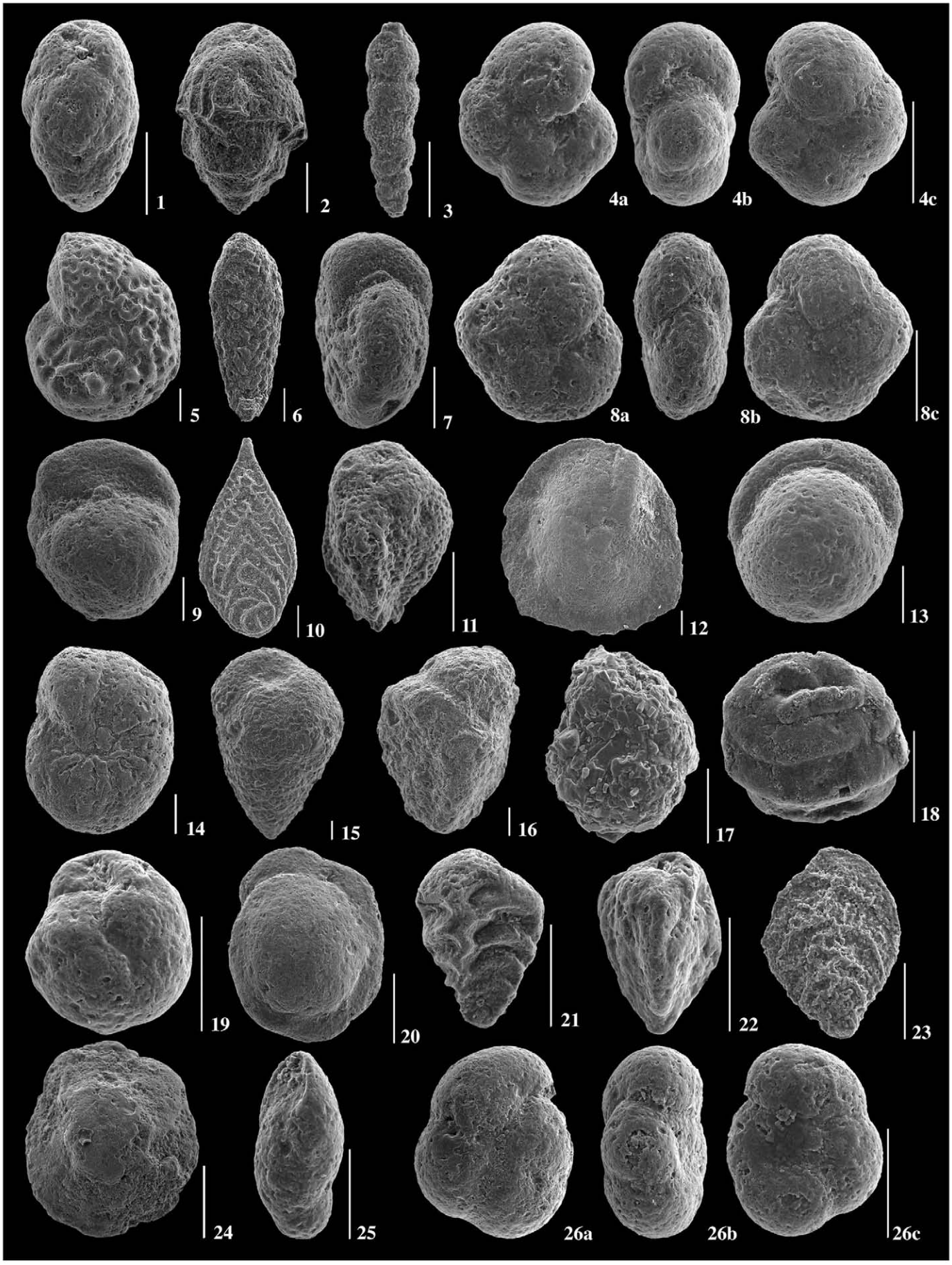
1
2
3
4a
4b
4c
5
6
7
8a
8b
8c
9
10
11
12
13
14
15
16
17
18
19
20
21
22
23
24
25
26a
26b
26c

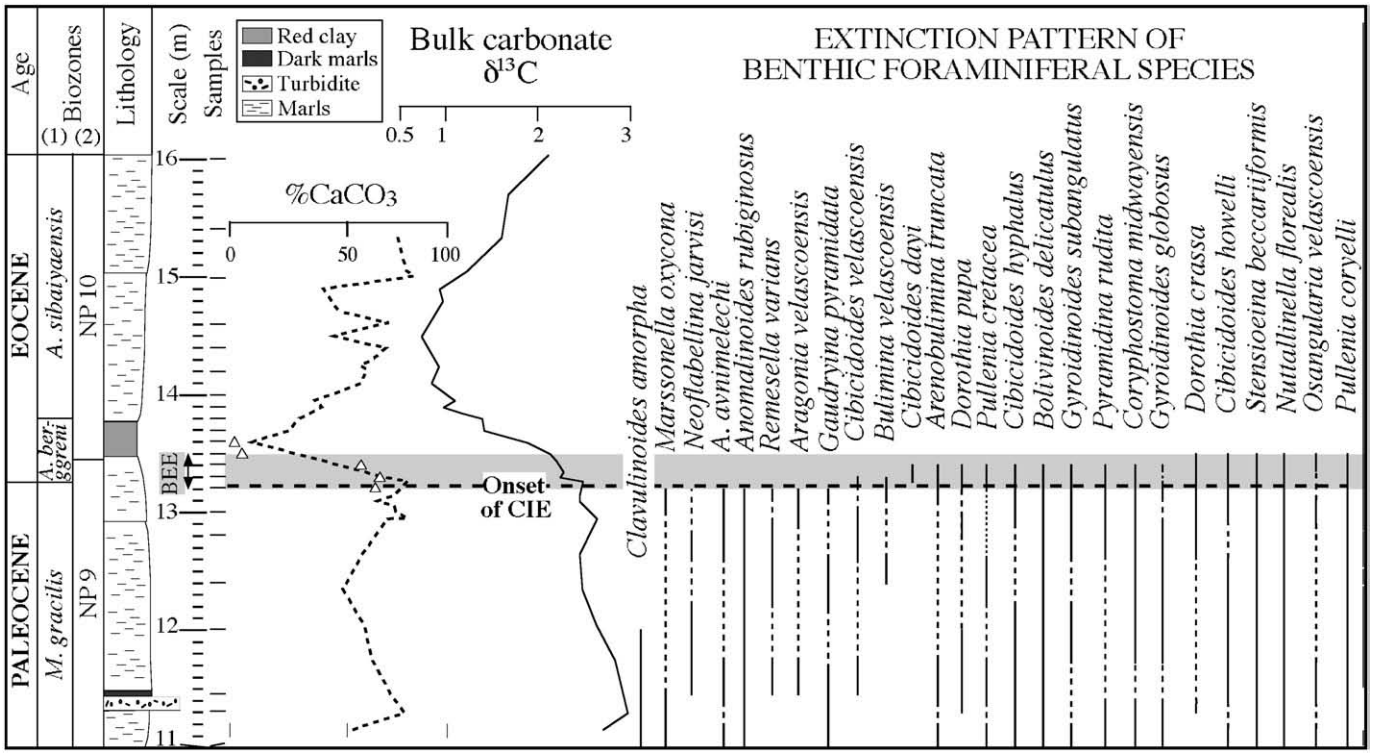

Fig. 5. Stratigraphic distribution of benthic foraminiferal taxa that disappear in the lowermost Eocene in Alamedilla, and correlation to the $\delta^{13}C$ curve (in bulk sediment) and calcite content (Lu et al., 1996). The 30-cm-thick interval of the BEE is shown in grey colour. White triangles represent the $\%CaCO_3$ analyses carried out across the critical BEE interval in this study. (1) Arenillas and Molina (1996) and Molina et al. (1999); (2) Monechi et al. (2000). *M.* = *Morozovella; A.* = *Acarinina*.

should also be pointed out that, since increased temperatures affect metabolic rates (Thomas, 2007), the same amount of food at higher temperatures would result in a more oligotrophic looking benthic foraminiferal assemblage. One might argue that the increased numbers of benthic foraminifera per gram of washed residue (Fig. 2) indicates increased food supply to the seafloor (e.g., Herguera and Berger, 1991; Jorissen et al., 1995). Nevertheless, we cannot say whether the total benthic biomass increased or decreased because the abundance of benthic foraminifera may be balanced by the small size of the tests, as documented from other lowermost Eocene assemblages (Thomas, 2007). High numbers of the calcareous nannofossil *Coccolithus pelagicus* have been documented within this interval (samples 13.80 to 14) at Alamedilla (Monechi et al., 2000), coeval with a unique opportunistic planktic foraminiferal assemblage (compressed acarininids; Lu et al., 1996, 1998; Arenillas and Molina, 1996). However, these studies do not provide strong interpretations as to increased or decreased productivity in surface waters.

The carbonate dissolution interval and the $CaCO_3$-undersaturated bottom waters inferred after the BEE might be related to the release of methane and shoaling of the CCD (e.g., Dickens et al., 1997; Zachos

Plate I. Scanning electron-micrographs of the most significant upper Paleocene and lower Eocene benthic foraminiferal species at Alamedilla. All scale-bars represent 100 μm.

1. *Bulimina tuxpamensis* (meter 13.80).
2. *Bulimina trinitatensis* (meter 11.45).
3. *Siphogenerinoides brevispinosa* (meter 13.40).
4a–c. *Abyssamina quadrata* (meter 13.30).
5. *Anomalinoides rubiginosus* (meter 11.45).
6. *Bolivinoides delicatulus* (meter 13.20).
7. *Cibicidoides hyphalus* (meter 12).
8a–c. *Abyssamina* sp. (meter 15).
9. *Gyroidinoides globosus* (meter 13.20).
10. *Neoflabellina jarvisi* (meter 11.45).
11. *Pyramidina rudita* (meter 13.20).
12. *Osangularia velascoensis* (meter 11.45).
13. *Pullenia coryelli* (meter 11.45).
14. *Stensioeina beccariiformis* (meter 11.45).
15. *Arenobulimina truncata* (meter 13.20).
16. *Gaudyrina pyramidata* (meter 11.45).
17. trochamminid (meter 13.80).
18. *Repmanina charoides* (meter 13.60).
19. *Globocassidulina subglobosa* (meter 13.90).
20. *Oridorsalis umbonatus* (meter 14.90).
21. *Tappanina selmensis* (meter 13.80).
22. *Reusella terquemi* (meter 13.90).
23. *Aragonia aragonensis* (meter 14.40).
24. *Nuttallides truempyi* (meter 16).
25. *Pleurostomella* sp. (meter 14.40).
26a–c. *Quadrimorphina profunda* (meter 14.40).

et al., 2004; Zeebe and Zachos, 2007). A second interval of dissolution just below the CIE recovery interval has been observed in several bathyal and abyssal sections of central and western Tethys (e.g., Giusberti et al., 2009). At Alamedilla, we analysed in detail the preservation of benthic foraminifera across the main CIE interval, where a second marked drop in calcite and an increase in the percentage of silicate minerals were detected ~160 cm above the onset of the CIE by Lu et al. (1996). However, no evidence for strong dissolution of benthic foraminiferal tests has been observed at that level.

At Alamedilla, as in many other deep-water settings (e.g., Schmitz et al., 1997; Giusberti et al., 2007), the percentage of carbonate increases gradually up-section (Lu et al., 1996), which is consistent with the slow deepening of the CCD after an abrupt and rapid acidification of the oceans.

4.3. The recovery of the CIE

The uppermost part of the studied section includes the partial recovery (D–F; c.a. +71.25 to +94.23 ky) and stabilization (>+94.23 ky) of the bulk carbonate $\delta^{13}C$ (Figs. 2, 3), although the studied interval does not include the whole recovery phase of the bulk carbon $\delta^{13}C$ values (e.g., Röhl et al., 2007). A sharp decrease in sedimentation rates is recorded at metre ~15 (Fig. 4), coinciding with the decreased percentage of silicate minerals and stabilization of the carbonate content (Fig. 2). Benthic foraminiferal assemblages in this part of the section are stable and consist of mixed infaunal and epifaunal morphogroups, reflecting mesotrophic conditions and well-oxygenated sea-bottom waters.

5. Conclusions

The analysis of benthic foraminifera across the Paleocene–Eocene transition at the lower bathyal–upper abyssal Alamedilla section (SE Spain) allowed us to distinguish assemblages (pre-extinction fauna, extinction fauna, post-extinction disaster and post-extinction opportunistic fauna, and recovery fauna) with paleoenvironmental significance, and to associate them to different portions of the $\delta^{13}C$ curve. Provided the small initial shift in bulk $\delta^{13}C$ at Alamedilla is indeed coeval with the larger initial shift at Site 690, one could argue that the record is much more complete at Alamedilla, at least over the beginning of the CIE, making it one of the most complete marine records over that interval.

Upper Paleocene assemblages indicate deposition above the calcite compensation depth, and well-oxygenated bottom waters. The extinctions of benthic foraminifera started in coincidence with the onset of the CIE (+0 ky), over an interval with a high calcite content, and had a duration c.a. 10 ky. The exact causes of the extinctions are not clear, yet, but they are likely to be related to paleoecological and paleoenvironmental instability triggered by global warming.

Assemblages just above the BEE are strongly dominated by the disaster fauna (*Glomospira* Acme). The carbonate dissolution interval and the $CaCO_3$-undersaturated bottom waters inferred after the BEE might be related to the release of methane, which led to a drop in ocean pH and shoaling of the CCD.

During the core of the CIE, the disaster fauna was rapidly replaced by opportunistic taxa that point to oxic bottom waters undersaturated in calcium carbonate, and possibly, oligotrophic conditions at the seafloor, whereas there is no strong evidence for increased or decreased productivity in surface waters. The CCD gradually dropped during this interval, leading to improved preservation of calcareous benthic foraminiferal tests towards the recovery interval.

A recovery fauna is identified in coincidence with the recovery (D–F; c.a. +70 to +94.23 ky) and stabilization (>+94.23 ky) of the $\delta^{13}C$. Our results support a gradual but rapid onset of the PETM, followed by long-term effects on benthic foraminiferal assemblages.

Acknowledgements

We thank the reviewers E. Thomas and M. Kaminski, and the editor Th. Corrège, for their helpful comments which were material in improving the manuscript. We acknowledge the Spanish Ministerio de Ciencia y Tecnología and Fondo Social Europero for a "Ramón y Cajal" research contract to L. Alegret and a post-doctoral grant EX2007-1094 to S. Ortiz; this research was funded by project Consolider CGL 2007-63724.

References

Alegret, L., 2007. Recovery of the deep-sea floor after the Cretaceous/Paleogene boundary event: the benthic foraminiferal record in the Basque–Cantabrian basin and in South-eastern Spain. Palaeogeography, Palaeoclimatology, Palaeoecology 255, 181–194.

Alegret, L., Thomas, E., 2005. Cretaceous/Paleogene boundary bathayl paleo-environments in the central North Pacific (DSDP Site 465), the Northwestern Atlantic (ODP Site 1049), the Gulf of Mexico and the Tethys: the benthic foraminiferal record. Palaeogeography, Palaeoclimatology, Palaeoecology 224, 53–82.

Alegret, L., Thomas, E., 2007. Deep-sea environments across the Cretaceous/Paleogene boundary in the eastern South Atlantic Ocean (ODP Leg 208, Walvis Ridge). Marine Micropaleontology 64, 1–17.

Alegret, L., Molina, E., Thomas, E., 2001. Benthic foraminifera at the Cretaceous/Tertiary boundary around the Gulf of Mexico. Geology 29, 891–894.

Alegret, L., Molina, E., Thomas, E., 2003. Benthic foraminiferal turnover across the Cretaceous/Paleogene boundary at Agost (southeastern Spain): paleoenvironmental inferences. Marine Micropaleontology 48, 251–279.

Alegret, L., Ortiz, S., Arenillas, I., Molina, E., 2005. Paleoenvironmental turnover across the Paleocene/Eocene boundary at the stratotype section in Dababiya (Egypt) based on benthic foraminifera. Terra Nova 17, 526–536.

Alegret, L., Ortiz, S., Orue-Etxebarria, X., Bernaola, G., Baceta, J.I., Monechi, S., Apellaniz, E., Pujalte, V., 2009. The Paleocene–Eocene Thermal Maximum: new data from the microfossil turnover at Zumaia section. Palaios 24, 318–328.

Arenillas, I., Molina, E., 1996. Bioestratigrafía y evolución de las asociaciones de foraminíferos planctónicos del tránsito Paleoceno–Eoceno en Alamedilla (Cordilleras Béticas). Revista Española de Micropaleontología 28 (1), 75–96.

Bains, S.R., Corfield, R.M., Norris, R.D., 1999. Mechanisms of climate warming at the end of the Paleocene. Science 285, 724–727.

Bains, S.R., Norris, R.D., Corfield, R.M., Faul, K.L., 2000. Termination of global warmth at the Paleocene/Eocene boundary through productivity feedback. Nature 407, 171–174.

Berggren, W.A., Aubert, J., 1975. Paleocene benthonic foraminiferal biostratigraphy, paleobiogeography and paleoecology of Atlantic–Tethyan regions: midway-type fauna. Palaeogeography, Palaeoclimatology, Palaeoecology 18, 73–192.

Berggren, W.A., Pearson, P.N., 2005. A revised tropical to subtropical Paleogene planktonic foraminiferal zonation. Journal of Foraminiferal Research 35, 279–298.

Bolli, H.M., Beckmann, J.P., Saunders, J.B., 1994. Benthic Foraminiferal Biostratigraphy of the South Caribbean Region. Cambridge University Press, Cambridge, UK.

Boltovskoy, E., Scott, D.B., Medioli, F.S., 1991. Morphological variations of benthic foraminiferal tests in response to changes in ecological parameters, a review. Journal of Paleontology 65, 175–185.

Bowen, G.J., Clyde, W.C., Koch, P.L., Ting, S., Alroy, J., Tsubamoto, T., Wang, Y., Wang, Y., 2006. Mammalian dispersal at the Paleocene/Eocene boundary. Science 15, 2062–2065.

Bralower, T.J., 2002. Evidence for surface water oligotrophy during the Late Paleocene–Eocene Thermal Maximum: nannofossil assemblages data from Ocean Drilling Program Site 690, Maud Rise, Weddell Sea. Paleoceanography 17 (2), 1–12 10.1029/2001PA000662.

Corliss, B.H., 1985. Microhabitats of benthic foraminifera within deep-sea sediments. Nature 314, 435–438.

Corliss, B.H., 1991. Morphology and microhabitat preferences of benthic foraminifera from the northeast Atlantic Ocean. Marine Micropaleontology 17, 195–236.

Corliss, B.H., Chen, C., 1988. Morphotype patterns of Norwegian Sea deep-sea benthic foraminifera and ecological implications. Geology 16, 716–719.

Cramer, B.S., Kent, D.V., 2005. Bolide summer: the Paleocene/Eocene thermal maximum as a response to an extraterrestrial trigger. Palaeogeography, Palaeoclimatology, Palaeoecology 224 (1–3), 144–166.

Crouch, E.M., Heilmann-Clausen, C., Brinkhuis, H., Morgans, H.E.G., Rogers, K.M., Egger, H., Schmitz, B., 2001. Global dinoflagellate event associated with the late Paleocene thermal maximum. Geology 29 (4), 315–318.

Dickens, G.R., Castillo, M.M., Walker, J.C.G., 1997. A blast of gas in the latest Paleocene: simulating first-order effects of massive dissociation of oceanic methane hydrate. Geology 25 (3), 259–262.

Dickens, G.R., Fewless, T., Thomas, E., Bralower, T.J., 2003. Excess barite accumulation during the Paleocene/Eocene thermal maximum: massive input of dissolved barium from seafloor gas hydrate reservoirs. In: Wing, S.L., Gingerich, P.D., Schmitz, B., Thomas, E. (Eds.), Causes and Consequences of Globally Warm Climates in the Early Paleogene, Geological Society of America Special Publication, 369. Geological Society of America, Boulder, Colorado, pp. 11–23.

Egger, H., Homayoun, M., Huber, H., Rögl, F., Schmitz, B., 2005. Early Eocene climatic, volcanic, and biotic events in the northwestern Tethyan Untersberg section, Austria. Palaeogeography, Palaeoclimatology, Palaeoecology 217, 243–264.

Galeotti, S., Kaminski, M.A., Coccioni, R., Speijer, R., 2004. High resolution deep water agglutinated foraminiferal record across the Paleocene/Eocene transition in the Contessa Road Section (central Italy). In: Bubik, M., Kaminski, M.A. (Eds.), Proceedings of the Sixth International Workshop on Agglutinated Foraminifera: Grzybowski Foundation Special Publication, vol. 8, pp. 83–103.

Gibbs, S.J., Bralower, T.J., Bown, P.R., Zachos, J.C., Bybell, L., 2006. Shelf-open ocean calcareous phytoplankton assemblages across the Paleocene–Eocene Thermal Maximum: implications for global productivity gradients. Geology 34, 233–236.

Giusberti, L., Rio, D., Agnin, C., Backman, J., Fornaciari, E., Tateo, F., Oddone, M., 2007. Mode and tempo of the Paleocene–Eocene thermal maximum in an expanded section from the Venetian Pre-Alps. Geological Society of America Bulletin 119, 391–412.

Giusberti, L., Coccioni, R., Sprovieri, M., Tateo, F., 2009. Perturbation at the sea floor during the Paleocene–Eocene thermal maximum: evidence from benthic foraminifera at Contessa Road. Italy: Marine Micropaleontology 70 (3), 102–119.

Gupta, A.K., Thomas, E., 2003. Initiation of Northern Hemisphere glaciation and strengthening of the northeast Indian monsoon: Ocean Drilling Program Site 758, eastern equatorial Indian Ocean. Geology 31 (1), 47–50.

Hay, W.W., DeConto, R.M., Wold, C.N., Wilson, K.M., Voigt, S., Schulz, M., Rossby Wold, A., Dullo, W.C., Ronov, A.B., Balukhovsky, A.N., Söding, E., 1999. An alternative global Cretaceous paleogeography. In: Barrera, E., Johnson, C. (Eds.), Evolution of the Cretaceous Ocean/Climate System: Geological Society of America Special Paper, vol. 332, pp. 1–47.

Herguera, J.C., Berger, W.H., 1991. Paleoproductivity from benthic foraminifera abundance: glacial to postglacial change in the west-equatorial Pacific. Geology 19, 1173–1176.

Jones, R.W., Charnock, M.A., 1985. "Morphogroups" of agglutinated foraminifera. Their life positions and feeding habits and potential applicability in (Paleo)Ecological studies. Revue de Palèobiologie 4, 311–320.

Jorissen, F.J., De Stigter, H.C., Widmark, J.G.V., 1995. A conceptual model explaining benthic foraminiferal microhabitats. Marine Micropaleontology 22, 3–15.

Kaminski, M.A. 1988. Cenozoic deep-water agglutinated foraminifera in the North Atlantic. – Ph.D. Thesis, WHOI/MIT Joint Program in Oceanography. WHOI 88-3, pp. 262.

Kaminski, M.A., Gradstein, F., 2005. Atlas of Paleogene Cosmopolitan Deep-Water Agglutinated Foraminifera: Grzybowski Foundation Special Publication, vol. 10, pp. 1–548.

Kaminski, M.A., Kuhnt, W., Radley, J.D., 1996. Paleocene–Eocene deep water agglutinated foraminifera from the Numidian Flysch (Rift, Northern Morocco): their significance for the paleoceanography of the Gibraltar gateway. Journal of Micropaleontology 15, 1–19.

Katz, M.E., Pak, D.K., Dickens, G.R., Miller, K.G., 1999. The source and fate of massive carbon input during the latest Paleocene thermal maximum. Science 286, 1531–1533.

Katz, M.E., Cramer, B., Mountain, G.S., Katz, S., Miller, K.G., 2001. Uncorking the bottle: what triggered the Paleocene/Eocene methane release? Paleoceanography 16 (6), 549–562.

Kauffman, E.G., Harries, P.J., 1996. The importance of crisis progenitors in recovery from mass extinction. In: Hart, M.B. (Ed.), Biotic Recovery from Mass Extinction Events: Geological Society Special Publications London, vol. 102, pp. 15–39.

Kauffman, E.G., Harries, P.J., Hansen, T.A., 1996. Models of biotic survival following mass extinction. In: Hart, M.B. (Ed.), Biotic Recovery from Mass Extinction Events: Geological Society Special Publications London, vol. 102, pp. 41–60.

Kelly, D.C., Bralower, T.J., Zachos, J.C., 1998. Evolutionary consequences of the latest Paleocene thermal maximum for tropical planktonic foraminifera. Palaeogeography, Palaeoclimatology, Palaeoecology 141, 139–161.

Kennett, J.P., Stott, L.D., 1991. Abrupt deep-sea warming, palaeoceanographic changes and benthic extinctions at the end of the Palaeocene. Nature 353, 225–229.

Koch, P.L., Zachos, J.C., Gingerich, P.D., 1992. Correlation between isotope records in marine and continental carbon reservoirs near the Palaeocene/Eocene boundary. Nature 358, 319–322.

Lu, G., Keller, G., Adatte, T., Ortiz, N., Molina, E., 1996. Long-term (10^5) or short-term (10^3) $\delta^{13}C$ excursion near the Palaeocene–Eocene transition: evidence from the Tethis. Terra Nova 8, 347–355.

Lu, G., Adatte, T., Keller, G., Ortiz, S., 1998. Abrupt climatic, oceanographic and ecologic changes near the Paleocene–Eocene transition in the deep Tethys basin: the Alamedilla section, southern Spain. Ecoglae geol. Helvetiae 91, 293–306.

Ly, A., Kuhnt, W., 1994. Late Cretaceous benthic foraminiferal assemblages of the Casamanca Shelf (Senegal, NW Africa). Indication of a late Cretaceous Oxygen Minimum Zone. Revue de Micropaléontologie 37, 49–74.

Molina, E., Arenillas, I., Pardo, A., 1999. High resolution planktic foraminiferal biostratigraphy and correlation across the Palaeocene/Eocene boundary in the Tethys. Bulletin de la Société géologique de France 170 (4), 521–530.

Monechi, S., Angori, E., Von Salis, K., 2000. Calcareous nannofossil turnover around the Paleocene/Eocene transition at Alamedilla (southern Spain). Bulletin de la Société géologique de France 171 (4), 477–489.

Murray, J.W., 1991. Ecology and Paleoecology of Benthic Foraminifera. Longman, Harlow.

Ortiz, N., 1995. Differential patterns of benthic foraminiferal extinctions near the Paleocene/Eocene boundary in the North Atlantic and the western Tethys. Marine Micropaleontology 26 (1–4), 341–359.

Orue-Etxebarria, X., Apellaniz, E., Baceta, J.I., Coccioni, R., di Leo, R., Dinarés-Turrell, J., Galeotti, S., Monechi, S., Núñez-Betelu, K., Pares, J.M., Payros, A., Pujalte, V., Samso, J.M., Serra-Kiel, J., Schmitz, B., Tosquella, J., 1996. Physical and biostratigraphic analysis of two prospective Paleocene–Eocene boundary stratotypes in the intermediate-deep water Basque Basin, western Pyrenees: the Trabakua Pass and Ermua sections. Neues Jahrbuch für Geologie und Paläontologie, Abhanlugen 201, 179–242.

Pagani, M., Pedentchouk, N., Huber, M., Sluijs, A., Schouten, S., Brinkhuis, H., Sinninghe Damsté, J.S., Dickens, G.R., Expedition-Scientists, 2006. Arctic hydrology during global warming at the Palaeocene–Eocene thermal maximum. Nature 442 (7103), 671–675.

Pujalte, V., Orue-Etxebarria, X., Schmitz, B., Tosquella, J., Baceta, J.I., Payros, A., Bernaola, G., Caballero, F., Apellaniz, E., 2003. Basal Ilerdian (earliest Eocene) turnover of larger foraminifera: age constraints based on calcareous plankton and $\delta^{13}C$ isotopic profiles from new southern Pyrenean sections (Spain). In: Wing, S.L., Gingerich, P.D., Schmitz, B., Thomas, E. (Eds.), Causes and Consequences of Globally Warm Climates in the Early Paleogene: Geological Society of America, Special Paper, vol. 369, pp. 205–221.

Röhl, U., Bralower, T.J., Norris, G., Wefer, G., 2000. A new chronology for the late Paleocene thermal maximum and its environmental implications. Geology 28, 927–930.

Röhl, U., Westerhold, T., Bralower, T.J., Zachos, J.C., 2007. On the duration of the Paleocene–Eocene thermal maximum (PETM). Geochemistry, Geophysics, Geosystems 8, Q12002. doi:10.1029/2007GC001784.

Schmitz, B., Asaro, F., Molina, E., Monechi, S., von Salis, K., Speijer, R.P., 1997. High-resolution iridium $\delta^{13}C$, $\delta^{18}O$, foraminifera and nannofossil profiles across the latest Paleocene benthic extinction event at Zumaya, Spain. palaeogeography, Palaeoclimatology, Palaeoecology 133 (1–2), 49–68.

Shipboard Scientific Party, 2004. Explanatory notes. In: Zachos, J.C., Kroon, D., Blum, P., et al. (Eds.), Proc. ODP, Init. Repts., 208: College Station, TX (Ocean Drilling Program), pp. 1–63. doi:10.2973/odp.proc.ir.208.102.2004.

Sluijs, A., Bowen, G.J., Brinkhuis, H., Lourens, L.J., Thomas, E., 2007a. The Palaeocene–Eocene thermal maximum super greenhouse: biotic and geochemical signatures, age models and mechanisms of global change. In: Williams, M., Haywood, A.M., Gregory, F.J., Schmidt, D.N. (Eds.), Deep Time Perspectives on Climate Change: Marrying the Signal from Computer Models and Biological Proxies. The Micropaleontological Society, special publications. The Geological Society, London, pp. 323–349.

Sluijs, A., Brinkhuis, H., Schouten, S., Bohaty, S.M., John, C.M., Zachos, J.C., Reichart, G.J., Sinninghe Damste, J., Crouch, E.M., Dickens, G.R., 2007b. Environmental precursors to rapid light carbon injection at the Paleocene/Eocene boundary. Nature 450, 1218–1221.

Smart, C.W., Thomas, E., Ramsay, A.T.S., 2007. Middle–late Miocene benthic foraminifera in a western Indian Ocean Depth Transect: paleoceanographic implications. Palaeogeography, Palaeoclimatology, Palaeoecology 247, 402–420.

Steineck, P.L., Thomas, E., 1996. The latest Paleocene crisis in the deep sea: Ostracode succession at Maud Rise, Southern Ocean. Geology 24, 583–586.

Stoll, H.M., 2005. Limited range of interspecific vital effects in coccolith stable isotopic records during the Paleocene–Eocene thermal maximum. Paleoceanography 20 (PA1007). doi:10.1029/2004PA001046.

Suhr, S.B., Pond, D.W., 2006. Antarctic benthic foraminifera facilitate rapid cycling of phytoplankton-derived organic carbon. Deep-Sea Research II 53, 895–902.

Suhr, S.B., Pond, D.W., Gooday, A.J., Smith, C.R., 2003. Selective feeding by benthic foraminifera on phytodetritus on the western Antarctic Peninsula shelf: evidence from fatty acid biomarker analysis. Marine Ecology, Progress Series 262, 153–162.

Svensen, H., Planke, S., Malthe-Sorenssen, A., Jamtveit, B., Myklebust, R., Rasmussen-Eidem, T., Rey, S., 2004. Release of methane from a volcanic basin as a mechanism for initial Eocene global warming. Nature 429, 542–545.

Takeda, K., Kaiho, K., 2007. Faunal turnovers in central Pacific benthic foraminifera during the Paleocene–Eocene thermal maximum. Palaeogeography, Palaeoclimatology, Palaeoecology 251, 175–197.

Thomas, E., 1990. Late Cretaceous through Neogene deep-sea benthic foraminifers (Maud Rise, Weddell Sea, Antarctica). Proceedings of the Ocean Drilling Program Scientific Results 113, 571–594.

Thomas, E., 1998. The biogeography of the late Paleocene benthic foraminiferal extinction. In: Aubry, M.P., Lucas, S., Berggren, W.A. (Eds.), Late Paleocene–Early Eocene Biotic and Climatic Events in the Marine and Terrestrial Records. Columbia University Press, pp. 214–243.

Thomas, E., 2003. Extinction and food at the seafloor: a high-resolution benthic foraminiferal record across the Initial Eocene Thermal Maximum, Southern Ocean Site 690. In: Wing, S.L., Gingerich, P.D., Schmitz, B., Thomas, E. (Eds.), Causes and Consequences of Globally Warm Climates in the Early Paleogene: Geological Society of America Special Paper, vol. 369, pp. 319–332. Boulder, Colorado.

Thomas, E., 2007. Cenozoic mass extinctions in the deep sea; what disturbs the largest habitat on Earth? In: Monechi, S., Coccioni, R., Rampino, M. (Eds.), Large Ecosystem Perturbations: Causes and Consequences: Geological Society of America Special Paper, vol. 424, pp. 1–24.

Thomas, E., Shackleton, N.J., 1996. The Paleocene–Eocene benthic foraminiferal extinction and stable isotope anomalies. In: Knox, R.W., Corfield, R.M., Dunay, R.E. (Eds.), Correlation of the Early Paleogene in Northwest Europe: Geological Society of London Special Publication, vol. 101, pp. 401–441.

Tjalsma, R.C., Lohmann, G.P., 1983. Paleocene–Eocene bathyal and abyssal benthic foraminifera from the Atlantic Ocean. Micropaleontology, Special Publication 4, 1–90.

Tremolada, F., Bralower, T.J., 2004. Nannofossil assemblage fluctuations during the Paleocene–Eocene Thermal Maximum at Sites 213 (Indian Ocean) and 401 (North Atlantic Ocean): palaeoceanographic implications. Marine Micropaleontology 52 (1–4), 107–116.

Van Morkhoven, F.P.C.M., Berggren, W.A., Edwards, A.S., 1986. Cenozoic Cosmopolitan Deep-water Benthic Foraminifera: Bulletin des Centres de Recherche Exploration-Production Elf-Aquitaine. In: Memoir, vol. 11. Pau, France.

Westerhold, T., Rohl, U., Raffi, I., Fornaciari, E., Monechi, S., Reale, V., Bowles, J., Evans, H.F., 2008. Astronomical calibration of the Paleocene time. Palaeogeography, Palaeoclimatology, Palaeoecology 257 (4), 377–403.

Wing, S.L., Harrington, G.J., Smith, F.A., Bloch, J.I., Boyer, D.M., Freeman, K.H., 2005. Transient floral change and rapid global warming at the Paleocene–Eocene Boundary. Science 310 (5750), 993–996.

Zachos, J.C., Lohmann, K.C., Walker, J.C.G., Wise, S.W., 1993. Abrupt climate change and transient climates during the Palaeogene: a marine perspective. Journal of Geology 101, 191–213.

Zachos, J., Pagani, M., Sloan, L.C., Thomas, E., Billups, K., 2001. Trends, rhythms, and aberrations in global climate 65 Ma to Present. Science 292, 686–693.

Zachos, J.C., Kroon, D., Blum, P., et al., 2004. Proceedings of the Ocean Drilling Program, Initial Reports, 208. http://wwwodp.tamu.edu/publications/208_IR/208ir.htm.

Zachos, J.C., Röhl, U., Schellenberg, S.A., Sluijs, A., Hodell, D.A., Kelly, D.C., Thomas, E., Nicolo, M., Raffi, I., Lourens, L.J., McCarren, H., Kroon, D., 2005. Rapid acidification of the ocean during the Paleocene–Eocene Thermal Maximum. Science 308, 1611–1615.

Zeebe, E., Zachos, J.C., 2007. Reversed deep-sea carbonate ion basin gradient during Paleocene–Eocene thermal maximum. Paleoceanography 22, PA3201. doi:10.1029/2006PA001395.